

Evolutionary tracks of FR II sources through the P–D diagram

Christian R. Kaiser^{*}, Jane Dennett–Thorpe and Paul Alexander

MRAO, Cavendish Laboratory, Madingley Road, Cambridge CB3 0HE

10 October 1997

ABSTRACT

This is the second in a series of papers presenting an analytical model for the evolution of FR II radio sources. In this paper we evaluate the expected radio emission from a radio source incorporating energy loss processes for the relativistic electrons. By combining these results with our earlier dynamical model we calculate evolutionary tracks through the Power–Linear size diagram. These tracks are in good agreement with the observed distribution of sources in this diagram. The effects of different forms for the evolution of the magnetic field in the cocoon, the redshift of the source, the environment of the source and the defining parameters of the jet are investigated. The evolutionary tracks are found to be insensitive to the assumed form of the magnetic field evolution. Some evidence against protons as a major constituent of the jet material is also found.

Key words: Radiation mechanisms: cyclotron and synchrotron – Galaxies: active – Galaxies: jets

1 INTRODUCTION

This is the second in a series of papers presenting an analytical model for the evolution of FR II radio sources; in the first paper (Kaiser & Alexander 1997, hereafter KA97) we investigated the dynamical evolution of the source and here we extend this analysis to consider the luminosity evolution of a radio source and the tracks it follows through the Power–Linear size (P–D) diagram. The P–D diagram was introduced by Shklovskii (1963) as a powerful tool for investigating the temporal evolution of FRI and FR II radio sources. By plotting the radio luminosity at a specific frequency, P_ν , as a function of the linear size of a source, D , a diagram analogous to the Hertzsprung–Russel diagram is obtained. The evolution of a radio source through the P–D diagram is, however, not well understood. Some constraints can be placed on these evolutionary tracks by the relative densities of objects in regions of the P–D diagram; specifically, sources with large linear sizes ($D > 1$ Mpc) and high radio luminosities ($P_\nu > 10^{26}$ W Hz⁻¹ sr⁻¹ at $\nu = 178$ MHz) seem to be rather rare suggesting that the luminosity of sources should decrease quickly with linear size for sizes approaching 1 Mpc. Care must be taken in interpreting the P–D diagram in this way since selection effects have a strong influence on the observed high–redshift population (e.g. Masson 1980, Macklin 1982) and giant sources are likely to be difficult to detect since the extended emission of the cocoon will be

weak and the hot spots may therefore appear unconnected (e.g. Muxlow & Garrington 1991). Searches specifically for giants have been undertaken by Cotter *et al.* (1996) and Subrahmanyam *et al.* (1996). Both groups identify a number of radio sources in low frequency surveys as classical doubles of extreme size, although almost all of these sources have luminosities below 2×10^{26} W Hz⁻¹ sr⁻¹ suggesting that there is a real deficit of powerful giant sources.

Baldwin (1982) used the model for FR II sources of Scheuer (1974) and minimum energy arguments (e.g. Burbidge 1956) to calculate evolutionary tracks through the P–D diagram. In its original form his model predicts $P \propto D^{7/8}$ for a power law energy spectrum of the relativistic electrons, $N(E) dE \propto E^{-p} dE$, with $p = 2$ as exponent. This implies that all sources would crowd together in exactly that area of the diagram which is almost empty. Modifications of the model incorporating a density gradient in the external medium surrounding the radio source ($\rho_x \propto d^{-\beta}$, where d is the distance from the center of the distribution) predicted tracks with decreasing radio luminosity in reasonable agreement with observations for $\beta = 1.9$ and $D < 300$ kpc. To explain the rapid decline in luminosity for $D \approx 1$ Mpc Baldwin suggested that the density of the atmosphere may decrease more steeply with $\beta = 2.9$ for $D > 300$ kpc. However, sources in environments with a density gradient steeper than $1/d^2$ are unlikely to develop the typical FR II morphology (Falle 1991, Kaiser & Alexander 1997).

An alternative hypothesis to account for the decrease in luminosity at large D is that the central engine ceases

^{*} email: ckaiser@mrao.cam.ac.uk

to supply energy to the jet after a certain period which is similar for all sources (for a discussion see Daly 1994). The cocoon will then dim quickly via adiabatic expansion. Observations indicate that only of order 4% of all radio sources show no signs of ongoing AGN activity Giovannini (1988) in support of this hypothesis.

The synchrotron radiation of FRIIs demonstrates the presence of highly relativistic electrons in the cocoon (e.g. Rees 1971). To achieve charge neutrality in the cocoon we need some species of positively charged particles. If we assume that there is no entrainment across the contact discontinuity which is separating the cocoon from the IGM the jet must supply these additional particles. The nature of these charge-balancing particles is subject to debate (e.g. Leahy 1991). If they are protons, a significant fraction of the kinetic energy transported by the jet will be stored by these in the cocoon but will not contribute to the radiated power. Alternatively, if the particles providing charge neutrality were positrons, they would behave almost exactly like electrons in a completely tangled magnetic field and will contribute to the observed synchrotron emission. The kinetic power of the jet required to produce a cocoon of given radio luminosity would be significantly reduced in the case of a pair plasma.

In this paper we extend the model described in KA97 for FRII sources by the addition of energy loss processes of the relativistic electrons in the cocoon to compute evolutionary tracks through the P–D diagram. We show that changes in the external atmosphere or a mechanism for switching off the central engine are not required to reproduce the observed distribution of sources in the P–D diagram. We also find some evidence against protons as a major constituent of the jet material. In section 2 we discuss synchrotron emission, the energy loss processes of the relativistic electrons responsible for this emission and a model for the cocoon based on KA97 which allows us to calculate its radio emission. Section 3 contains a discussion of the results obtained with this model for the cocoon and examines changes to the evolutionary tracks through the P–D diagram introduced by different models for the evolution of the magnetic field in the cocoon, the redshift of the source, its orientation with respect to the line of sight and the addition of thermal, non-radiating particles to the material in the cocoon.

2 THE RADIO EMISSION OF THE COCOON

In this section we firstly present a brief review of the synchrotron emission mechanism and the energy losses affecting the relativistic electrons responsible for this emission. We will assume these electrons to be confined to a small volume element. We then go on to develop a model for the emissivity of the whole of the cocoon by summing up the contribution of each volume element. We neglect the emission of the hot spots since we are confining our interest in this paper to those radio sources in which the emission of the cocoon dominates the total radio luminosity of the source.

2.1 Synchrotron radiation and loss processes

The specific volume emissivity due to synchrotron radiation, j_ν , of an ensemble of relativistic electrons in a magnetic field

of energy density u_B averaged over all electron pitch angles is (e.g. Shu 1991):

$$j_\nu = \int_1^\infty \frac{4}{3} \sigma_T c u_B \beta_e^2 \gamma^2 \Phi(\nu, \gamma) n(\gamma) d\gamma, \quad (1)$$

where σ_T is the Thompson cross section, c the speed of light, β_e the speed of the relativistic electrons in units of c ($\beta_e \approx 1$), γ the corresponding Lorentz factor and $n(\gamma) d\gamma$ the number density of electrons with Lorentz factors between γ and $\gamma + d\gamma$. Taking the average over all possible electron pitch angles is justified since we assume that the magnetic field is completely tangled on scales much smaller than the cocoon itself. The spectral emission of an electron of Lorentz factor γ is given by $\Phi(\nu, \gamma)$. In this paper we are primarily concerned with the total source luminosity, rather than details of spectral shape and therefore we use the standard approximation that electrons are emitting only at their critical frequency $\nu = \gamma^2 \nu_L$, where ν_L is the Larmor frequency; this allows us to set $\Phi(\nu, \gamma) = \delta(\nu - \gamma^2 \nu_L)$. Taking the electron ensemble to occupy a volume V the emitted radio power per unit frequency and solid angle is

$$P_\nu = \frac{1}{6\pi} \sigma_T c u_B \frac{\gamma^3}{\nu} n(\gamma) V. \quad (2)$$

If the relativistic electrons are initially accelerated at time t_i (for example via a first order Fermi process at the jet shock) we expect their energy distribution to be a power law function of their initial Lorentz factor, γ_i , (e.g. Heavens & Drury 1988)

$$n(\gamma_i, t_i) d\gamma_i = n_o \gamma_i^{-p} d\gamma_i. \quad (3)$$

This spectrum will then evolve with time as the electron population loses internal energy. The rate of change of the Lorentz factor for the electron population is given by

$$\frac{d\gamma}{dt} = -\frac{a_1}{3} \frac{\gamma}{t} - \frac{4}{3} \frac{\sigma_T}{m_e c} \gamma^2 (u_B + u_C). \quad (4)$$

The first term on the right hand side represents adiabatic expansion losses for the case where the volume V expands as $V \propto t^{a_1}$ (e.g. Longair 1981). The second term is the combined loss rate due to synchrotron radiation and inverse Compton scattering of the cosmic microwave background radiation (CMBR); m_e is the electron mass and u_C is the energy density of the CMBR. Integration of equation (4) gives

$$\frac{t^{-\frac{a_1}{3}}}{\gamma} - \frac{t_i^{-\frac{a_1}{3}}}{\gamma_i} = \frac{4}{3} \frac{\sigma_T}{m_e c} \int_{t_i}^t (u_B + u_C) (t')^{-\frac{a_1}{3}} dt', \quad (5)$$

where for an electron with a Lorentz factor of γ at time t , the Lorentz factor at time t_i , when it was initially accelerated, is γ_i , and we may therefore consider γ_i to be a function of γ and t . As mentioned above we assume the magnetic field to be completely tangled on all relevant scales, allowing us to treat u_B as a pressure with adiabatic index, Γ_B , such that $u_B \propto t^{-\Gamma_B a_1}$. The energy density of the CMBR, u_C , is a function of redshift ($u_C \propto (z+1)^4$), but since the lifetime of radio sources does not exceed a few times 10^8 years (Alexander & Leahy 1987) we take u_C to be constant during the evolution of a given source. Performing the integral in equation (5):

$$\frac{t^{-\frac{a_1}{3}}}{\gamma} - \frac{t_i^{-\frac{a_1}{3}}}{\gamma_i} = a_2(t, t_i), \quad (6)$$

where

$$a_2(t, t_i) = \frac{4\sigma_T}{3m_e c} \times \left[\frac{u_B(t_i)}{a_3} t_i^{a_1 \Gamma_B} (t^{a_3} - t_i^{a_3}) + \frac{u_C}{a_4} (t^{a_4} - t_i^{a_4}) \right], \quad (7)$$

with $a_3 = 1 - a_1(\Gamma_B + 1/3)$ and $a_4 = 1 - a_1/3$. If $u_e(t_i)$ is the energy density of the relativistic electrons at time t_i , we find for $n_o(t_i)$ from equation (3)

$$n_o = \frac{u_e(t_i)}{m_e c^2} \left(\int_{\gamma_{i,min}}^{\gamma_{i,max}} (\gamma_i - 1) \gamma_i^{-p} d\gamma_i \right)^{-1} = \frac{u_e(t_i)}{m_e c^2} \left(\frac{\gamma_{i,min}^{2-p} - \gamma_{i,max}^{2-p}}{p-2} - \frac{\gamma_{i,min}^{1-p} - \gamma_{i,max}^{1-p}}{p-1} \right)^{-1}, \quad (8)$$

where $\gamma_{i,min}$ and $\gamma_{i,max}$ are the low and high energy cut-off of the initial energy distribution. The electrons are uniformly distributed over the volume V . Because of the expansion of V we have to set $t^{\alpha_1} n(\gamma, t) d\gamma = t_i^{\alpha_1} n(\gamma_i, t_i) d\gamma_i$. Thus the energy distribution of the relativistic electrons at time t can be shown to be

$$n(\gamma, t) d\gamma = n_o \frac{\gamma_i^{2-p}}{\gamma^2} \left(\frac{t}{t_i} \right)^{-\frac{4a_1}{3}} d\gamma, \quad (9)$$

where from equation (6)

$$\gamma_i = \frac{\gamma t_i^{-\frac{a_1}{3}}}{t^{-\frac{a_1}{3}} - a_2(t, t_i) \gamma} \quad (10)$$

and n_o is given by equation (8).

2.2 A model for the cocoon

The overall dynamics of the cocoon, and specifically the evolution of the cocoon pressure, p_c , were considered in detail in KA97; in this section we review the essentials of this model necessary to calculate the luminosity of the source and to determine also how an element of radio emitting plasma evolves within the cocoon.

For the calculation of the radio emission of the cocoon we divide its contents into three separate ‘fluids’ with individual energy densities. The first fluid consists of the electrons (and possibly positrons); these are described by the energy spectrum given in equation (3) and contribute an energy density u_e with adiabatic index Γ_e . For a completely tangled field we have a magnetic ‘fluid’ with energy density u_B and adiabatic index, $\Gamma_B = 4/3$. Finally, we allow for the possibility that protons and/or electrons with a thermal spectrum are present in the cocoon with an energy density u_T and adiabatic index Γ_T . The overall dynamics are governed by the pressure in the cocoon, $p_c = (\Gamma_c - 1)(u_e + u_B + u_T)$; where the adiabatic index of the cocoon as a whole, Γ_c , depends on the relative pressures of each component.

To allow for variations of the energy densities within the cocoon we split the cocoon into small volume elements δV . The fluid present in the volume δV is injected into the cocoon at a time t_i over a short time interval δt_i , during which the internal energy of δV , δU , changes according to

$$d(\delta U) = Q_o d(\delta t_i) - p_c(t_i) d(\delta V), \quad (11)$$

where Q_o is the power of the jet. During the interval δt_i the volume elements expand adiabatically which changes their pressure from the hot spot pressure $p_h(t_i)$ to that of the cocoon $p_c(t_i + \delta t_i) \approx p_c(t_i)$. With this assumption integration of equation (11) gives

$$\delta U = \frac{p_c(t_i) \delta V(t_i)}{\Gamma_c - 1} = Q_o \delta t_i - \frac{p_c(t_i) \delta V(t_i)}{\Gamma_c - 1} \left[\left(\frac{p_h(t_i)}{p_c(t_i)} \right)^{\frac{\Gamma_c - 1}{\Gamma_c}} - 1 \right]. \quad (12)$$

From KA97 we take $p_h/p_c \approx 4R^2$ which then yields

$$\delta V(t_i) = \frac{(\Gamma_c - 1) Q_o}{p_c(t_i)} (4R^2)^{\frac{1-\Gamma_c}{\Gamma_c}} \delta t_i. \quad (13)$$

If the expansion of δV after the interval δt_i is also adiabatic we finally find

$$\delta V(t) = \frac{(\Gamma_c - 1) Q_o}{p_c(t_i)} (4R^2)^{\frac{1-\Gamma_c}{\Gamma_c}} \left(\frac{t}{t_i} \right)^{a_1} \delta t_i, \quad (14)$$

where $a_1 = (4 + \beta)/(\Gamma_c(5 - \beta))$. Here we have used the result from KA97 that $p_c \propto t^{(-4-\beta)/(5-\beta)}$ with β being the exponent in the density distribution of the external atmosphere.

We define k' as the ratio of the energy densities of the thermal particles, u_T , to that of the electrons, u_e , when they are injected into the cocoon at t_i . Note that this differs from the usual way of defining k as the ratio of the energy densities of non-radiating particles and relativistic electrons. In our case the non-relativistic electrons of the power law energy distribution (equation 9) are already included in u_e . We also introduce r as the ratio of the energy density of the magnetic field, u_B , to the sum of the energy densities of the particles, $u_e + u_T$. With these definitions:

$$u_e(t_i) = \frac{p_c(t_i)}{(\Gamma_c - 1)(k' + 1)(r + 1)}, \quad u_B(t_i) = \frac{r p_c(t_i)}{(\Gamma_c - 1)(r + 1)}. \quad (15)$$

By identifying V in equation (2) with δV we can calculate the radio emission of this volume element, and obtain the total emission of the cocoon by summing the contributions of all such elements within the cocoon; from equation (14) it is clear that this sum reduces to an integration over the injection time, t_i :

$$P_\nu = \int_0^t \frac{\sigma_T c r}{6\pi \nu (r + 1)} Q_o n_o (4R^2)^{\frac{1-\Gamma_c}{\Gamma_c}} \times \frac{\gamma^{3-p} t_i^{\frac{a_1}{3}(p-2)}}{\left(t^{-\frac{a_1}{3}} - a_2(t, t_i) \gamma \right)^{2-p}} \left(\frac{t}{t_i} \right)^{-a_1(\frac{1}{3} + \Gamma_B)} dt_i. \quad (16)$$

For the older parts of the cocoon the energy losses of the relativistic electrons can be so severe that $\gamma_i \rightarrow \infty$ in equation (10), i.e. electrons with the correct Lorentz factor, γ , to produce radiation with frequency ν now, at time t , would have had $\gamma_i \rightarrow \infty$ at injection time, t_i . Volume elements for which this is the case no longer contribute to the radio emission, hence we define a minimum injection time,

t_{min} , at which the cocoon material is still radiating at frequency ν . The integration limits in equation (16) are then from t_{min} to t .

The integral in equation (16) is not analytically soluble for arbitrary p , and we therefore use a numerical approach, the results of which we present in Section 3.

3 EVOLUTIONARY TRACKS

To perform the calculations discussed in section 2 an explicit form for the electron distribution function at the time the electrons are injected into the cocoon is required. It is shown in KA97 that the material in the jet is ‘cold’ implying an adiabatic index of 5/3. Nevertheless, in the rest frame of the jet shock the jet material is moving at relativistic speeds ($0.77c \rightarrow 0.87c$ for the parameters used in KA97), which implies an exponent for the energy distribution of $p = 2.14$ (Heavens & Drury 1988). This value is derived using a test particle approach which may not be appropriate for jet shocks in extragalactic sources. However, the spectral indices of observed radio sources infer $2 \leq p \leq 3$ (e.g. Alexander & Leahy 1987) and we therefore use $p = 2.14$ for the tracks calculated in this section. Since $p > 2$, all moments of the electron energy distribution up to the second moment (related to the synchrotron loss rate) are insensitive to the choice of upper limit for the energy distribution, $\gamma_{i,max}$, and specifically converge even as $\gamma_{i,max} \rightarrow \infty$; we therefore take this limiting value. The main form in which energy is transported along the jet is as bulk kinetic energy; the energy transported per particle in the jet is therefore approximately constant. The acceleration process at the jet shock transfers this energy to the fraction of the electron population constituting the power law energy distribution; a substantial proportion of the material in the cocoon must therefore be cold, contributing to the density but not the energy density. So as to account for this population we assume the power law distribution extends to $\gamma_{i,min} = 1$; however we shall for the moment neglect any thermal plasma setting $k' = 0$.

From KA97 we have expressions for the cocoon pressure p_c (assuming cylindrical symmetry of the cocoon) and for the linear size as a function of time ($D \propto t^{3/(5-\beta)}$). For the initial ratio of the energy densities of the magnetic field and of the particles we use $r = (1+p)/4$ which is taken from minimum energy arguments (e.g. Burbidge 1956). Other typical observational parameters are taken as follows. For the density profile of the external atmosphere ($\rho_x = \rho_o(d/a_o)^{-\beta}$) we take the central density $\rho_o = 7.2 \cdot 10^{-22} \text{ kg/m}^3$, for a core radius $a_o = 2 \text{ kpc}$ and $\beta = 1.9$; these values are typical for a galaxy out to about 100 kpc from its center (Canizares *et al.* 1987). Rawlings & Saunders (1991) find jet powers, Q^{rs} , from 10^{37} W to 10^{39} W for FR II sources. These authors used in their calculations a form of the minimum energy argument with cut-offs for the power law energy distribution corresponding to the observational limits of the radio spectrum of 10 MHz and 100 GHz respectively implying that there is no thermal material present in the cocoon ($k = 0$). Their frequency cut-offs translate in our model to $\gamma_{i,min} \sim 500$ and $\gamma_{i,max} \sim 10^5$ for a source with $D = 100 \text{ kpc}$. Since in our model the power law of the energy distribution extends to $\gamma_{i,min} = 1$ there is some thermal material present in the

cocoon and for the quoted values we find $k = 3.6$. We must therefore adjust their values to be consistent with our choice of $\gamma_{i,min}$ and $\gamma_{i,max}$. Rawlings & Saunders (1991) also assumed that half of the energy that is transported by the jet during its life time, t , is lost to the surrounding IGM because of the expansion work of the cocoon. However from KA97 we find that this work is given by

$$\int p_c dV_c = \frac{5 - \beta}{9[\Gamma_c + (\Gamma_c - 1)R^2] - 4 - \beta} Q_o t, \quad (17)$$

where V_c is the volume of the cocoon. We can therefore derive jet kinetic powers from the values given by Rawlings & Saunders (1991) using

$$\begin{aligned} Q_o &= \frac{9[\Gamma_c + (\Gamma_c - 1)R^2] - 4 - \beta}{10 - 2\beta} (k + 1)^{\frac{4}{5+p}} Q^{rs} \\ &\approx 13 Q^{rs}, \end{aligned} \quad (18)$$

where $R = 2$, $k = 3.6$ and $\Gamma_c = 5/3$.

The pressure in the cocoon also depends on its axial ratio, R , and the bulk velocity in the jet, v_j . We adopt $R = 2$ which is an average value (Leahy & Williams 1984) and $v_j = 0.87c$ implying a Lorentz factor of the bulk motion of $\gamma_j = 2$. This velocity is a rather arbitrary choice since there are no reliable estimates of v_j in the literature.

The distribution of sources in the P–D diagram is constructed from the data presented by Laing *et al.* (1983), Subrahmanyam *et al.* (1996) and Cotter *et al.* (1996); these authors quote luminosities at or close to an observing frequency of 178 MHz and we therefore use this frequency in our calculations. Note that the distribution of observed sources presented here cannot be taken as the ‘true’ distribution because of the involved selection effects. The observed linear size of a radio source projected onto the plane of the sky, D , depends of course not only on the advance speed of the hot spots but also on $\sin \alpha$, where α is the angle between the jet axis and the line of sight. Assuming that the low-frequency LRL sample represents a uniform distribution in α we adopt the average viewing angle $\alpha = 39.5^\circ$ for the model sources.

3.1 Evolution of the magnetic field

To proceed we need to know the equation of state of the material in the cocoon as a whole and also how the magnetic field is behaving during the expansion of the volume elements δV . Since there is a mixture of three different fluids in the cocoon this is not straight forward, and it is also likely that the equation of state varies both within the cocoon and with time. Hence we investigate three limiting cases:

- Case 1: Both, the cocoon and the magnetic field energy density, have a relativistic equation of state ($\Gamma_c = \Gamma_B = 4/3$).
- Case 2: The cocoon is ‘cold’ ($\Gamma_c = 5/3$) but the energy density of the magnetic field is proportional to the one of the relativistic particles and therefore $\Gamma_B = 4/3$.
- Case 3: Cocoon and magnetic field are ‘cold’ ($\Gamma_c = \Gamma_B = 5/3$). This implies some energy dissipation process between the magnetic field and the non-relativistic particles by which the adiabatic index of the energy density of the magnetic field is held constant at 5/3. This effectively keeps

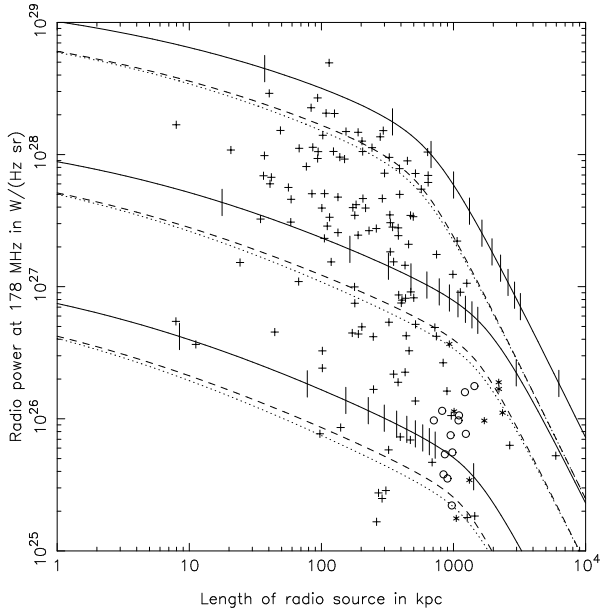


Figure 1. Evolutionary tracks for three FR II sources. The upper curves are for $Q_o = 1.3 \cdot 10^{40}$ W and $z = 2$, the curves in the center for $Q_o = 1.3 \cdot 10^{39}$ W and $z = 0.5$ and the lower curves for $Q_o = 1.3 \cdot 10^{38}$ W and $z = 0.2$. The other parameters for all sets of curves are: $R = 2$, $\rho_o = 7.2 \cdot 10^{-22}$ kg/m³, $a_o = 2$ kpc, $\beta = 1.9$ and $k' = 0$. Solid curves for case 1, dashed curves for case 2 and dotted curves for case 3 (see text). The vertical lines on the solid curves are time markers. The first marker on the left indicates a life time of 10^6 years of the respective source model. Next ten markers for every 10^7 years up to 10^8 years. At the last marker the source is $2 \cdot 10^8$ years old. Crosses are observed sources above 10^{25} W Hz⁻¹ sr⁻¹ taken from Laing et al. (1983), stars from Subrahmanyan et al. (1996) and circles from Cotter et al. (1996).

the energy of the magnetic field and that of the particles in equipartition.

In cases 1 and 3 the ratio of the energy densities of the magnetic field and of the particles for every volume element δV in the cocoon, $r = 0.785$ for the value of $p = 2.14$ adopted here, is not changing with time. In case 2 the value of r will increase with time since the adiabatic index of the magnetic field is lower than the one of the particles. This implies that after some time the energy density of the magnetic field will start to dominate the total energy density in δV and therefore change the adiabatic index of this part of the cocoon. For a volume element injected into the cocoon at time t_i the ratio of energy densities r becomes equal to 1 at time $t \approx 1.9 \cdot t_i$. At the same time the total volume of the cocoon, V_c , has increased by a factor 6.4 ($V_c \propto t^{9/(5-\beta)}$, see KA97) implying that in most parts of the cocoon $r < 1$. We therefore make the approximation that the adiabatic index of the cocoon as a whole is $5/3$.

Figure 1 shows the evolutionary tracks for all three cases (corrected for $\Gamma_c = 5/3$: $Q_o = 13 \cdot Q^{rs}$) for two limiting jet powers $Q_o = 1.3 \cdot 10^{38}$ W and $Q_o = 1.3 \cdot 10^{40}$ W and an intermediate case with $Q_o = 1.3 \cdot 10^{39}$ W; the redshift z is 0.2 for the low power jet, 0.5 for the ‘average’ jet and 2 for the high power jet.

The range of luminosities observed in FR II sources is bounded by the tracks for the two limiting jet powers and

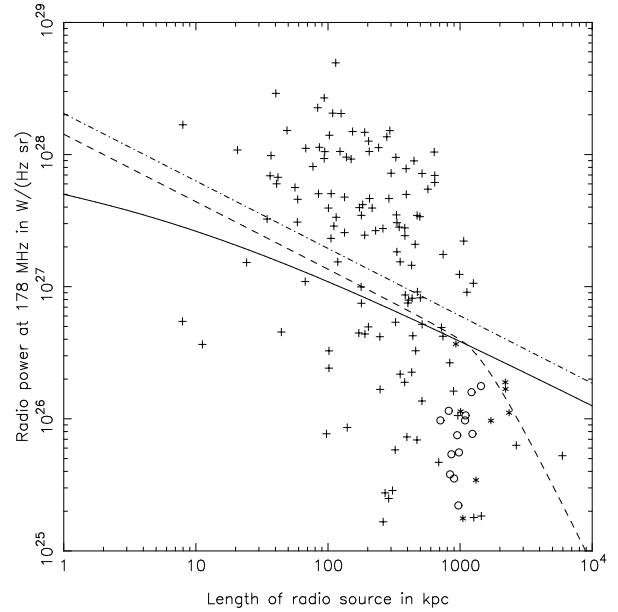


Figure 2. Comparison of the different loss processes. All model parameters as for the intermediate case in figure 1. The energy loss processes of the relativistic electrons considered are different for the tracks: Solid curve: adiabatic losses plus synchrotron losses, dashed: adiabatic losses plus inverse Compton losses, dot-dashed: no losses.

the drop in luminosity caused by the catastrophic energy losses of the relativistic electrons occurs at approximately the correct linear size. The importance of radiative losses in reducing the source luminosity at large linear sizes (even at a low observing frequency) is very significant — the lack of large (Mpc) sources at high luminosity is therefore a direct result of their intrinsic luminosity evolution, and is a strong function of frequency. Most of the observed sources ‘crowd’ in the region of the diagram between 100 kpc and 1 Mpc. From the time markers on the tracks in figure 1 it is clear that the model discussed here predicts exactly this behaviour since model sources spend the longest part of their life time in this region of the diagram. The difference between cases 2 and 3 is almost negligible. The higher luminosity for case 1 results from the fact that in this case less of the energy transported by the jet is lost in the expansion of the cocoon. Using the appropriate correction factor for Q_o for this case by setting $\Gamma_c = 4/3$ in equation (18), which yields $Q_o = 2.3 \cdot Q^{rs}$, puts this track very close to the other two. Thus we can conclude that the different possibilities for the equation of state of the cocoon and for the evolution of the magnetic field do not have a significant influence on the evolutionary tracks. We will therefore use only case 3 in the following.

Figure 2 shows a comparison of the effects of the various loss processes. The most luminous track in this figure represents a model where the energy losses of the relativistic electrons are completely neglected, i.e. the right hand side of equation (4) is set to zero. This curve is equivalent to the results of Baldwin (1982). The two other tracks shown both incorporate adiabatic losses plus one of the radiative loss processes each. Obviously the adiabatic losses lead to a pure luminosity off-set which one would expect from equation (4) if the two radiative terms on the right are set to zero.

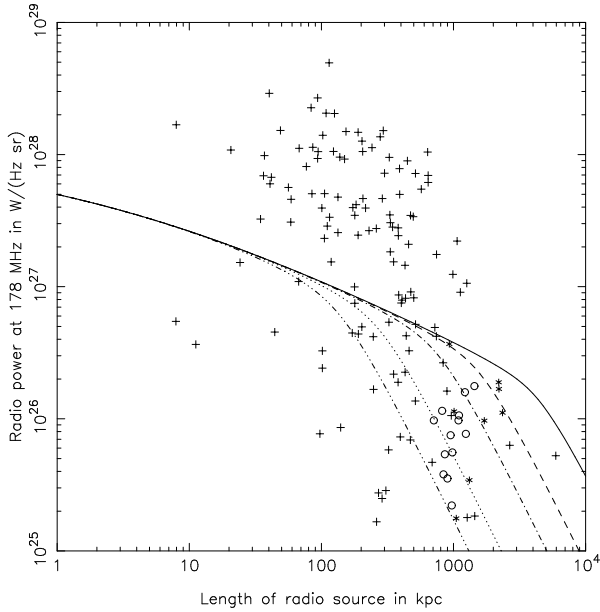


Figure 3. The influence of the redshift z on the evolutionary tracks at $\nu = 178$ MHz. Solid curve: $z = 0$, dashed: $z = 0.5$, dot-dashed: $z = 1$, dotted: $z = 2$ and dot-dot-dot-dashed: $z = 3$. All other model parameters as in the intermediate case in figure 1.

From the figure it is also clear that synchrotron losses are dominating the shape of the track for small sources and inverse Compton losses are responsible for the steep decline of the luminosity of large sources. The decreasing importance of synchrotron losses with increasing linear size is caused by the decreasing energy density of the magnetic field in the cocoon. Once the energy density of the CMBR becomes comparable to the energy density of the magnetic field the inverse Compton losses determine the shape of the track and limit the size of the radio source.

As the source luminosity decreases as the result of inverse Compton losses, so the prominence of the hot spots will increase. A detailed investigation of this effect requires a proper model for the hot spot itself and will be investigated in a forthcoming paper.

3.2 Effects of redshift and environment

In figure 3 we show evolutionary tracks at an observing frequency of 178 MHz at various redshifts; the other source parameters are given in the figure caption. These tracks are calculated assuming that there is no evolution of the surrounding gas with redshift. Since the energy density of the CMBR increases with redshift the inverse Compton losses become important earlier and the evolutionary tracks begin to steepen for smaller linear sizes of the source.

The environments of radio sources have a great influence on their appearance. The effects on the radio luminosity of a source caused by a change in the shape of the density profile is shown in Figure 4, where the exponent, β , in the density distribution of the IGM is varied. The track for $\beta = 0$ is purely hypothetical since KA97 have pointed out that a jet with the parameters used here could not reach a linear size greater than about 80 kpc in a uniform environment

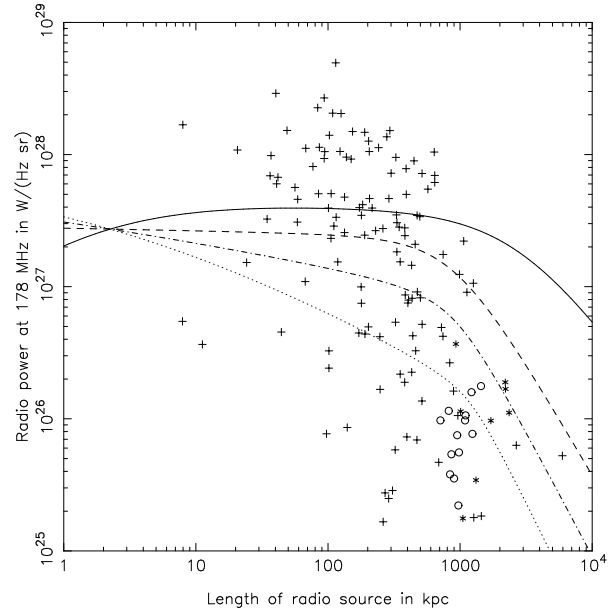


Figure 4. The influence of the shape of the density distribution in the IGM. Solid curve: $\beta = 0$, dashed: $\beta = 1$, dot-dashed: $\beta = 1.5$ and dotted: $\beta = 2$. All other model parameters as in the intermediate case in figure 1.

without being destroyed by turbulence; for this value of β the track is increasing in radio luminosity for small sources, a result also found by Baldwin (1982), but the inverse Compton losses are still strong enough to reverse this trend and cause the track to steepen for large linear sizes. The behaviour for $\beta = 1$ is close to that of a source with constant radio luminosity in the absence of radiative losses.

The point of intersection is due to the intrinsic characteristic time scale of the problem $\tau = (a_o^5 \rho_o / Q_o)^{1/3}$ (see KA97) which is the same for all values of β . Note also that the point at which inverse Compton losses become important shifts to smaller linear sizes for smaller values of β (with the exception of $\beta = 0$). This is because the pressure in the cocoon is lower at any given linear size in the case of large values of β compared to smaller values. The population of relativistic electrons in these cases has therefore lost less energy when the energy density of the CMBR becomes comparable to the energy density of the magnetic field in the cocoon. The steepening of the track due to inverse Compton losses then occurs at larger linear sizes. In the case of $\beta = 0$ the luminosity of the source would increase with linear size for all sizes without any radiative losses. However, the synchrotron losses of the electrons in this case are so severe that the luminosity of the source is almost entirely produced by material which has just been injected into the cocoon while older parts are not radiating anymore, leading to almost constant radio luminosity for all linear sizes. Because of this the exact point at which inverse Compton losses become important in this case is difficult to determine and the start of the steepening of the track is less obvious.

The observed distribution of sources in the P-D diagram seems to be fitted best by tracks with β just less than 2. This is in agreement with $\beta = 1.9$ found by Cotter (1996), who constructed evolutionary tracks through the P-D diagram by comparing the positions of sources with similar

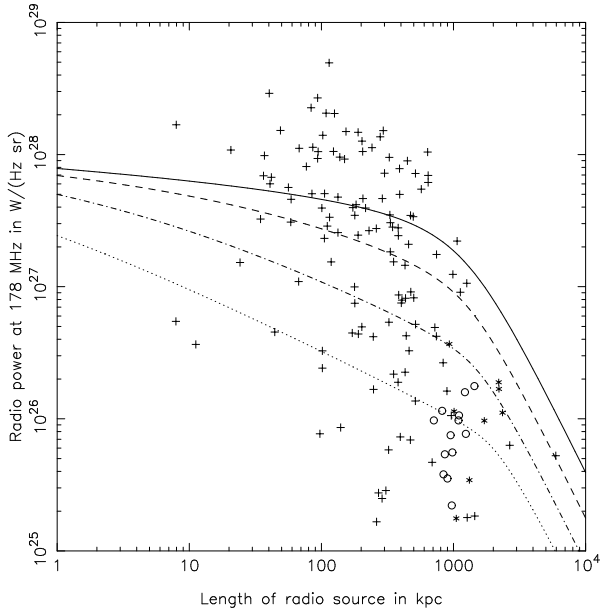


Figure 5. The influence of the central density of the density distribution of the IGM. Solid curve: $\rho_o = 7.2 \cdot 10^{-20} \text{ kg/m}^3$, dashed: $\rho_o = 7.2 \cdot 10^{-21} \text{ kg/m}^3$, dot-dashed: $\rho_o = 7.2 \cdot 10^{-22} \text{ kg/m}^3$ and dotted: $\rho_o = 7.2 \cdot 10^{-23} \text{ kg/m}^3$. All other parameters as in the intermediate case in figure 1.

observed jet power, and also with X-ray observations of the gas surrounding galaxies at low redshift (Canizares *et al.* 1987).

Figure 5 shows the effect of varying the central density of the IGM, ρ_o . For a greater central density the pressure in the cocoon is higher which leads to an increased radio luminosity and also to greater energy losses of the relativistic electrons via synchrotron radiation. This effect ‘flattens’ the tracks of small sources in a high density environment. Again the steepening of the tracks of large sources occurs at smaller linear sizes for sources in denser environments since their hot spot advance speeds are smaller.

3.3 Effects of jet properties

In section 3.1 we have already investigated the influence of the jet power, Q_o , on the evolutionary tracks. Other jet parameters which have an effect on the radio luminosity of radio sources are the jet half-opening angle, θ , (which controls the aspect ratio of the cocoon R) and the nature of the jet material.

If the expansion of the cocoon perpendicular to the jet axis is confined by the ram pressure of the IGM we find that the aspect ratio of the cocoon is determined by the ratio of the pressure at the hot spot to the pressure in the cocoon. From KA97 we find that this ratio is proportional to the inverse square of the jet half opening angle θ . Figure 6 shows the evolutionary tracks for the range of R observed in sources at constant Q_o . The limiting cases $R = 1.3$ and $R = 6$ correspond to $\theta = 47.8^\circ$ and $\theta = 10.4^\circ$ respectively. The pressure in the cocoon must be higher in the sources with wider cocoons to allow the faster expansion perpendicular to the jet axis, leading to higher synchrotron losses and hence giving relatively flat tracks for small linear sizes. Since the

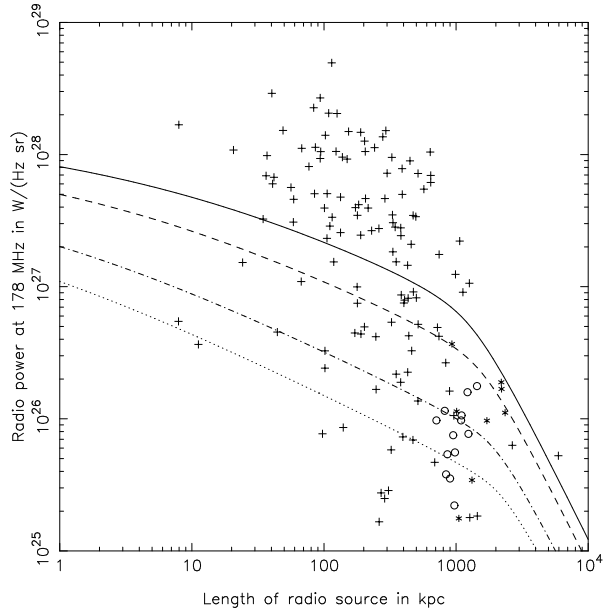


Figure 6. The influence of the aspect ratio of the cocoon R . Tracks are plotted for $Q_o = 1.3 \cdot 10^{39} \text{ W}$, $\rho_o = 7.2 \cdot 10^{-22} \text{ kg/m}^3$, $a_o = 2 \text{ kpc}$, $\beta = 1.9$, $k' = 0$ and $z = 0.5$. Solid curve: $R = 1.3$, dashed: $R = 2$, dot-dashed: $R = 4$ and dotted: $R = 6$.

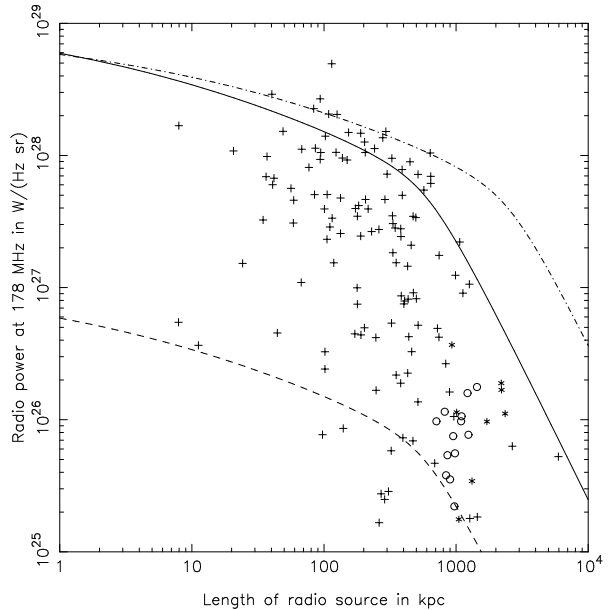


Figure 7. The influence of protons in the jet. Tracks are plotted for $\rho_o = 7.2 \cdot 10^{-22} \text{ kg/m}^3$, $a_o = 2 \text{ kpc}$, $\beta = 1.9$, $z = 2$ and $R = 2$. Solid curve: $Q_o = 1.3 \cdot 10^{40} \text{ W}$ and $k' = 0$, dashed: $Q_o = 1.3 \cdot 10^{40} \text{ W}$ and $k' = 100$ and dot-dashed: $Q_o = 10^{42} \text{ W}$ and $k' = 100$.

energy density at the hot spots is lower relative to that of the cocoons, the hot spot advance speeds are smaller than those for the sources with thinner cocoons and the steepening of the tracks occurs at smaller linear sizes.

All models considered up to this point have assumed that the jets consist of an electron–positron plasma and that the contribution of the thermal particles to the energy density in the cocoon is negligible. If there are protons in the jet they are also accelerated to relativistic velocities at the

jet shock. Bell (1978) showed that for an proton–electron plasma accelerated in a shock front the protons can store ten times more energy than the electrons. Other acceleration scenarios predict much higher values (Eilek & Hughes 1991). From figure 7 it is clear that an addition of protons to the jet material, even if they contribute only moderately to the energy density in the cocoon ($k' = 100$), decreases the luminosity of radio sources severely. Should the jets in FR II sources consist of protons and electrons they must have much higher energy transport rates than we have assumed so far in order to explain the most luminous sources. This would considerably increase the hot spot advance speeds of these sources and lead in turn to very large linear sizes for the sources before inverse Compton losses become significant (see figure 7). Since we do not observe such large luminous sources this can be taken as evidence against the presence of protons in the jet.

4 CONCLUSIONS

A model for the cocoon of FR II radio sources based on the model of KA97 is presented. Energy loss processes for the relativistic electrons producing the radio emission of the cocoon are incorporated into a calculation of the expected radio luminosity. The resulting evolutionary tracks through the P–D diagram are shown to be in good agreement with the observed distribution of sources. The lack of luminous giants in the diagram is reproduced just by the energy losses of the electrons without invoking changes in the density distribution of the IGM or the switching off of the central engine. The exact details of the evolution of the magnetic field in the cocoon are shown to have no significant effect on the evolutionary tracks. The effects of the environment and jet parameters on the tracks are investigated. The requirement of very high jet powers and the associated high hot spot advance speeds for proton–electron jets to account for the most luminous observed sources might rule out large fractions of protons in the jet.

ACKNOWLEDGEMENTS

We thank the referee Dr. J. P. Leahy for helpful comments on the manuscript.

REFERENCES

- Alexander P., Leahy J. P., 1987, MNRAS, 225, 1
 Baldwin J. E., 1982, in Heeschen D. S., Wade C. M., eds, Extragalactic radio sources. Reidel, p. 21
 Bell A. R., 1978, MNRAS, 182, 443
 Burbidge G. R., 1956, ApJ, 124, 416
 Canizares C. R., Fabbiano G., Trinchieri G., 1987, ApJ, 312, 503
 Cotter G., Rawlings S., Saunders R., 1996, MNRAS, 281, 1081
 Cotter G., 1996, PhD thesis, University of Cambridge
 Daly R. A., 1994, ApJ, 426, 38
 Eilek J. A., Hughes P. A., 1991, in Hughes P. A., ed, Beams and jets in astrophysics. Cambridge University Press, p. 428
 Falle S. A. E. G., 1991, MNRAS, 250, 581
 Giovannini G., Feretti L., Gregorini L., Parma P., 1988, A&A, 199, 73
 Heavens A. F., O’C. Drury L., 1988, MNRAS, 235, 997
 Kaiser C. R., Alexander P., 1997, MNRAS, 286, 215 [KA97]
 Laing R. A., Riley J. M., Longair M. S., 1983, MNRAS, 204, 151
 Leahy J. P., Williams A. G., 1984, MNRAS, 210, 929
 Leahy J. P., 1991, in Hughes P. A., ed, Beams and jets in astrophysics. Cambridge University Press, p. 100
 Longair M. S., 1981, High energy astrophysics. Cambridge University Press
 Macklin J. T., 1982, MNRAS, 199, 1119
 Masson C. R., 1980, ApJ, 242, 8
 Muxlow T. W. B., Garrington S. T., 1991, in Hughes P. A., ed, Beams and jets in astrophysics. Cambridge University Press, p. 52
 Rawlings S., Saunders R., 1991, Nat., 349, 138
 Rees M. J., 1971, Nat., 229, 312
 Scheuer P. A. G., 1974, MNRAS, 166, 513
 Shklovskii I. S., 1963, Sov. Astr., 6, 465
 Shu F. H., 1991, The physics of astrophysics. Vol.1: Radiation. University Science Books
 Subrahmanyam R., Saripalli L., Hunstead R. W., 1996, MNRAS, 279, 257